A Universal Grid-forming Inverter Model and Simulation-based Characterization Across Timescales

D. Ramasubramanian , E. Farantatos
Electric Power Research Institute
dramasubramanian, efarantatos@epri.com

O. Ajala
University of Illinois at Urbana-Champaign
ooajala2@illinois.edu

S. Dhople
University of Minnesota
sdhople@umn.edu

B. Johnson
University of Washington
brianbj@uw.edu

Abstract

The evolution of the power grid has given rise to a variety of innovations in inverter control architectures. Among these advances, a class of controllers has emerged with the aim of enabling 100% inverter-based grids and these are known as grid-forming methods. Since these strategies are still under active development, well validated models are needed by equipment manufacturers as well as system planners and operators. In particular, a system operator may be unable to determine specifications and services that are required from grid forming devices without having the ability to represent them in a simulation environment with trusted models. A universal grid forming model that is portable across multiple simulation domains will be valuable in addressing this issue. In this paper, we develop a practical implementation of such a model that has the ability to represent four different grid-forming methods in a variety of simulation software packages while accurately capturing dynamics across from microsecond to millisecond timescales.

1. Introduction

In a conventional power system paradigm, almost all inverter control architectures generally follow the same hierarchy of control loops and functional elements. While the intellectual property of each individual inverter manufacturer is still maintained, a generic model of such an inverter control scheme can still be derived by joining outer active power and reactive power control loops along with an inner current control and phase locked loop [1]. It goes without saying that the exact structure and parameters of these individual control loops is not expected to be the same across different manufacturers, but the functional performance is expected to be similar. Control architectures that are based on controlled power and current injections that follow the measured terminal voltage are known as *grid following (GFL)*. However, the evolution of the power grid both at the distribution and the transmission system levels has given rise to many different forms of new inverter control architectures. These new control architectures [2] have been given the moniker of *grid forming (GFM) control*.

Unlike synchronous machines whose initial transient and dynamic behavior is governed by Lenz's law of electromagnetism and Newton's laws of motion [3], an inverter's initial transient and dynamic behavior is largely governed by its digital control architecture. As a result, it can be a laborious task to develop generic mathematical simulation models that can cater to the various flavors of grid forming controls. Since inverter control algorithms are proprietary in nature, 'black box' or 'user-defined' simulation models are generally provided by the original equipment manufacturer (OEM) and such an approach can be expected even for grid forming inverters. While these models have the advantage of higher accuracy, there can be computational difficulties associated with the use of hundreds of distinct user defined models when studying a large system [1].

To reduce the burden on both simulation software developers as well as power system planners and operators, there is a need for a universal model that can capture the trend of the response of different grid forming inverter types. Furthermore, guidelines regarding the use of the universal model in terms of its parameterization across different time scales and simulation environments are required. Until recently, as the system strength of many large power systems was considered to be sufficiently strong for inverter current injection, positive sequence models were suitable for use in planning studies. However,

This material is based upon work supported by the U.S. Department of Energy's Office of Energy Efficiency and Renewable Energy (EERE) under Solar Energy Technologies Office (SETO) Agreement Numbers EE0009025 and EE0002437. The views expressed herein do not necessarily represent the views of the U.S. Department of Energy or the United States Government.

URI: https://hdl.handle.net/10125/102956
978-0-9981331-6-4

as the short circuit strength of the system reduces, not only do conventional inverter plants have an increased possibility of experiencing instability, but, state-of-the-art positive sequence models may lose numerical stability and fidelity. As a result, a system planner may be hindered in the use of positive sequence simulation tools to obtain a picture of the system dynamic behavior.

Presently, detailed electromagnetic transient (EMT) simulation studies which use black box models provided by IBR OEMs are being performed in systems where low system strength issues have been observed either in simulation or in the field. However, for large systems, running stability and contingency analysis on EMT simulation platforms can bring about a significant case preparation & computational burden [4]. With emerging inverter controls, the industry would benefit greatly from a universal model that can adequately represent this emerging inverter behavior in low short circuit conditions.

In this paper, the development of such a universal grid forming inverter model is discussed. The need and value of such a universal generic model can be questioned, especially for emerging technology which can still be considered to be very much in the research realm. However, at the same time, many equipment manufacturers may still be developing and finalizing their control methods, and in order to efficiently carry out this task, they need directions from system planners and operators. But, a system planner/operator may be unable to determine specifications and services that are required from grid forming devices without having the ability to represent a trend of the dynamic behavior of these devices in their studies. It is in this space that a generic model can help. A generic model of grid forming inverters for use in transmission and distribution planning analysis is vendor agnostic, but can be parameterized to provide the general trend of response of different types of grid forming controls.

There are research articles that discuss the intricacies of a specific GFM control type [5, 6, 7, 8]. Further, [9] provides a unified grid forming structure that spans only droop and virtual synchronous generator while [10] provides a grid forming structure of droop control that spans across EMT and phasor simulation domain. While these research efforts do represent the state of the art, our proposed effort extends the unified model to include more variety of GFM control architectures across simulation domains. Recent work has resulted in a generic structure for few GFM control architectures [11], but to the authors' knowledge, a universal generic model that spans both EMT domain and positive sequence domain, *and* spans more variety of GFM control architecture has so far not been proposed and developed for practical industry use. This paper aims to address this gap along with providing insight into the associated parameterization of the model. A detailed small signal stability analysis is carried out to identify the stability profile of the GFM control methods for different loading levels. Furthermore, the translation of the model from EMT domain to positive sequence domain is also highlighted. Such a translation will allow for its wide-spread use across large power systems while maintaining numerical fidelity and robustness. Case studies that showcase the applicability of using different grid forming control structures in the same network are developed.

The remainder of this paper is structured with Section 2 illustrating the operational similarity of a phase locked loop based GFM method with other conventional GFM methods. With this basis, a universal model is developed. Simulation results are then discussed in Section 3 and concluding remarks are provided in Section 4.

2. Universal Grid Forming Inverter Model

Grid forming inverters comprise a primary control and inner control loops. The primary control loops establish the steady-state relations between the inverter output power, voltage magnitude, and frequency. The inner control loops are responsible for limiting the output current of the inverter, as well as ensuring that the output voltage of the inverter tracks the values specified by the primary control.

In recent work [11], a generalized primary control structure across three different forms of grid forming control methods (i.e. virtual synchronous machine (VSM), droop, and dispatchable virtual oscillator (dVOC)) [5, 6, 7] has been developed. Structural similarities in these forms of GFM control allow for the development of a common control topology whose behavior mimics each primary grid forming control type through appropriate parameterization. In this section, we will describe how this generalized structure can be expanded to accommodate a grid forming approach that uses a modified phase locked loop (PLL) [12]. This expansion subsequently allows for the development of a universal model that can behave both in GFL and in GFM mode based on the parameterization. With appropriate parameterization and auxiliary control loops, each of the GFM control modes can additionally also provide black start services. Further, an intermediate GFL mode (I-GFL) is also possible wherein the GFL resource provides grid

support services such as frequency and voltage response, but is still unable to operate at extreme low short circuit conditions.

2.1. Modification of phase locked loop control to bring about grid forming property

When compared to the behavior of general primary GFM control structures from [11], a PLL based inverter control can also exhibit similar operational characteristics with appropriately designed auxiliary control loops. Further, many of these auxiliary control loops are either already present today in inverter control topologies, or the need has already been established in many grid requirements [13]. These section outlines the structure of these auxiliary control loops.

Traditionally, PLL based inverter controls are linked to grid following control architectures which control the output active and reactive power to the reference values of power P_{inv}^{ref} and Q_{inv}^{ref}. An intermediate GFL (I-GFL) control structure can incorporate an active power - frequency droop loop using the frequency evaluated by the PLL (ω_{PLL}) along with a droop gain of ω_{Drp}. However reactive power is still controlled to a reference value of Q_{inv}^{ref}. In some I-GFL structures, a coordinated Q-V control can be implemented along with droop gain of Q_{Drp}, but since the overall control objective is still to control reactive power to a reference value, the operational behavior is still dominated by grid following properties [14, 15, 16].

To allow an I-GFL control structure to exhibit grid forming properties, the following modifications can be implemented: (i) complete control of inverter terminal voltage to a reference value of V_{inv}^{ref} instead of reactive power control, (ii) droop on voltage control with a gain of Q_{Drp}, and (iii) power oscillation damper (POD) with PLL frequency (ω_{PLL}) as an input. Since other properties of the I-GFL structure are retained, it is assumed that droop based active power - frequency control (with droop gain ω_{Drp}) is also implemented at the inverter level [17]. The modified voltage control loop and active power control loop generate corresponding reference currents I_d^{ref} and I_q^{ref}. The resulting set of equations that define this operational similarity can be written as given in the set of equations (1)-(10). Here, s_x denotes a state variable whose index x denotes the quantity while $\dot{s}_x$ denotes the differential of the state variable with respect to time.

$$\dot{s}_\omega = K_{ipll} v_q \tag{1}$$

$$\dot{s}_\theta = s_\omega + K_{ppll} v_q + \omega_0 \tag{2}$$

$$\dot{s}_{i_d} = K_{ip}^{inv}\left(P_{inv}^{ref} - P_{inv} - \omega_{Drp}\left(s_\omega + K_{ppll} v_q\right)\right) \tag{3}$$

$$I_d^{ref} = s_{i_d} + K_{pp}^{inv}\begin{pmatrix} P_{inv}^{ref} - P_{inv} \\ -\omega_{Drp}\left(s_\omega + K_{ppll} v_q\right)\end{pmatrix} \tag{4}$$

$$\dot{s}_{i_q} = K_{iv}^{inv}\begin{pmatrix} V_{inv}^{ref} - v_d + Q_{Drp}\left(Q_{inv}^{ref} - Q_{inv}\right) \\ + K_{iv_q}^{inv} v_q + o_{2,pod}\end{pmatrix} \tag{5}$$

$$I_q^{ref} = s_{i_q} + K_{pv}^{inv}\begin{pmatrix} V_{inv}^{ref} - v_d \\ + Q_{Drp}\left(Q_{inv}^{ref} - Q_{inv}\right) \\ + K_{pv_q}^{inv} v_q + o_{2,pod}\end{pmatrix}. \tag{6}$$

Here, K_{ppll} and K_{ipll} denote the PLL control gains while K_{pp}^{inv} and K_{ip}^{inv} denote the active power control loop gains. The voltage control loop gaines are denoted by K_{pv}^{inv} and K_{iv}^{inv} while v_d and v_q denote the *dq* reference frame components of the inverter terminal voltage. Additionally here, the gains K_{pv}^{inv} and K_{iv}^{inv} hold negative values to account for the orientation of the dq and xy frames of reference. The *dq* reference frame is assumed to be aligned with the network reference frame at the angle θ generated by the generic primary control. Gains K_{pv_q} and K_{iv_q} are additional gains in the voltage control loop for the v_q component. The signal $o_{2,pod}$ represents the output of a POD.

A POD is a control loop which behaves in a manner similar to power system stabilizers in synchronous machines and brings about an increase in damping behavior. For an inverter based resource, although POD for active power have been proposed in literature, a POD in the reactive power - voltage control path is easier to design and implement [18, 19]. Using a conventional washout and lead-lag design, the equations of the POD can described as,

$$T_{w_{pod}}\dot{s}_{1,pod} = -K_{pod}\left(s_\omega + K_{ppll} v_q + \omega_0\right) - s_{1,pod} \tag{7}$$

$$o_{1,pod} = K_{pod}\left(s_\omega + K_{ppll} v_q + \omega_0\right) + s_{1,pod} \tag{8}$$

$$T_{2_{pod}}\dot{s}_{2,pod} = \left(1 - \frac{T_{1_{pod}}}{T_{2_{pod}}}\right) o_{1,pod} - s_{1,pod} \tag{9}$$

$$o_{2,pod} = \frac{T_{1_{pod}}}{T_{2_{pod}}} o_{1,pod} + s_{2,pod} \tag{10}$$

where K_{pod} and $T_{w_{pod}}$ represent the washout gain and time constant of the POD and $T_{1_{pod}}$ and $T_{2_{pod}}$ represent the lead-lag time constants.

An inner current control loop is used to control the current injected by the inverter (i_d, i_q) into the grid through a filter (L_f^1). Here, for simplicity, only the inductive portion of the output filter is considered.

The inner current control loop can be represented by the equations (11)-(14),

$$\dot{s}_{u_d^{ctrl}} = K_{ii}\left(I_d^{ref} - i_d\right) \tag{11}$$

$$u_d^{ctrl} = s_{u_d^{ctrl}} + K_{pi}\left(I_d^{ref} - i_d\right) \tag{12}$$

$$\dot{s}_{u_q^{ctrl}} = K_{ii}\left(I_q^{ref} - i_q\right) \tag{13}$$

$$u_q^{ctrl} = s_{u_q^{ctrl}} + K_{pi}\left(I_q^{ref} - i_q\right) \tag{14}$$

where u_d^{ctrl} and u_q^{ctrl} respectively represent the control effort along the *d* and *q* axis respectively.

With these modifications added to a conventional PLL based inverter control, it is now possible to construct a universal model of a grid forming inverter which can cater to multiple different control structures and time scales. Here, with appropriate parameterization, the universal model is expected to behave in a similar manner across different control structures.

2.2. Development of universal model

A universal model can now be developed which can be parameterized to represent a GFL operation mode, an I-GFL operation mode, and a GFM operation mode with each of the different types of primary control. A schematic block diagram of this universal model is as shown in Fig. 1. Each of the different operation modes can be toggled through parameterization of V_{flag}, Q_{flag}, ω_{flag}, and the droop gains ω_{Drp} and Q_{Drp}. The values for these elements are tabulated in Table 1. Here, for both droop gains, a generic value of K is tabulated, but the actual value can be based on the specific scenario being studied.

This universal model can be represented in both electromagnetic transient (EMT) domain and positive sequence domain. When representing the model in EMT domain, three phase instantaneous voltage ($V_{a,b,c}$) and current ($I_{a,b,c}$) on the grid side of filter L_f^1 are inputs to the control loops while the outputs are three phase instantaneous quantities ($E_{a,b,c}$) which denote the voltage generated by the inverter (in an average model).

When representing the model in positive sequence domain, few simplifications are required. Positive sequence simulation tools assume a balanced three phase network with the network impedance represented at fundamental frequency (ω_0) and voltages and currents represented as phasors. As a result, inputs to the control loops are now values of voltage and current on an $\alpha\beta$ rotating frame (i.e. v_α and v_β, i_α and i_β). Now, within the control loop, instead of representing a complete $abc \Rightarrow dq$ frame transformation, only an $\alpha\beta \Rightarrow dq$ rotating frame transformation is required which can be represented as,

$$\begin{aligned} v_d &= v_\alpha \cos(\theta) + v_\beta \sin(\theta), \\ v_q &= -v_\alpha \sin(\theta) + v_\beta \cos(\theta), \end{aligned} \tag{15}$$

where θ is the inverter's internal angle, from (2). A similar frame transformation is to be carried out on the input current variables. The output of the control loop is evaluated as e_d and e_q and transformed back to the $\alpha\beta$ frame at the network boundary. Additionally, in most commercially available positive sequence simulation platforms, time domain dynamic behavior of elements are evaluated through a solution methodology that numerically integrates differential equations sequentially with algebraic equations of the network [20]. This is in contrast to most EMT simulation platforms where, as network dynamics are also represented by differential equations, all equations can be solved simultaneously. As a result, in positive sequence domain to maintain numerical stability at the boundary buses (buses that separate the differential equations and algebraic equations), at the time of occurrence of a disturbance, an additional network convergence routine is to be incorporated into the inverter model [21].

The context of the universal model is therefore the ability to have one model with which the behavior of different control structures can be represented. Results from the implementation of the model in EMT domain, positive sequence time domain, and small signal domain will now be discussed in the following section.

Table 1. Flag settings in the universal model to bring about GFL, I-GFL, and GFM operation modes (see Fig. 1)

IBR Behavior	Control Type	V_{flag}	Q_{flag}	ω_{flag}	ω_{Drp}	Q_{Drp}
GFL	Qcntrl	N/A	0	0	0	0
	QVcntrl	1	1	0	0	0
I-GFL	Qcntrl	N/A	0	0	K	K
	QVcntrl	1	1	0	K	K
GFM	PLL	0	1	0	K	K
	VSM	N/A	N/A	1	K	K
	Droop	N/A	N/A	2	K	K
	dVOC	N/A	N/A	3	K	K

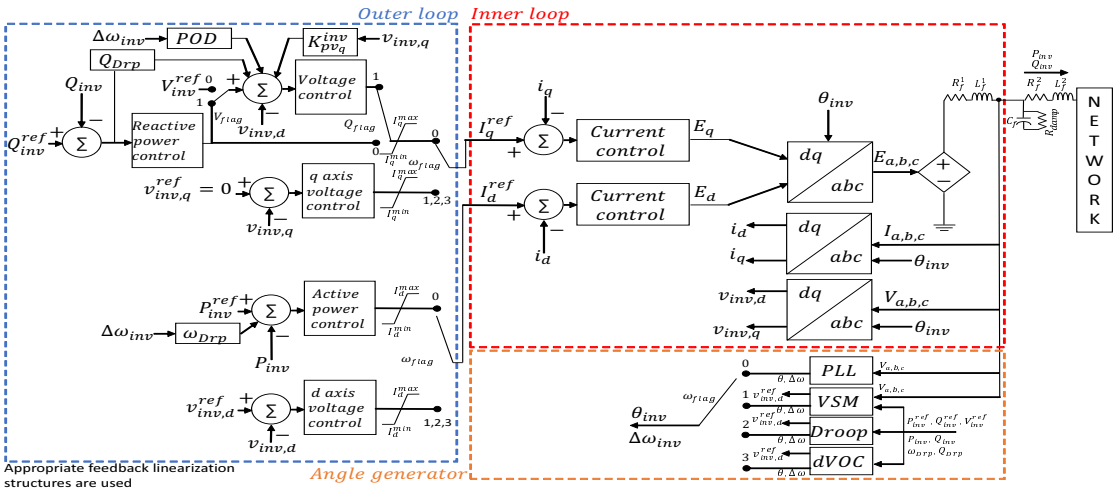

Figure 1. Schematic layout of universal control structure for a future inverter

3. Simulation Results

Through the use of a small signal state space model, operational similarity between the modified PLL based grid forming control topology and a droop based grid forming control topology is first discussed in this section. Subsequently, time domain simulation results comparing the behavior of the universal model across different time domains will be illustrated. Following this, the response of using various types of grid forming control methods in a larger system and comparison of the performance across simulation domains will be discussed. Small signal analysis results are obtained through linearization of the equations using Python similar to the approach described in [15]. However, due to space constraints, we don't explicitly show the derivation of the state space equations in this paper. Positive sequence time domain simulations are carried out in the GE-PSLF simulation solver with an integration time step of 1ms while EMT simulations are carried out in the PSCAD simulation solver with an integration time step of 5 μs.

3.1. Verification of structure and operational similarity

To verify the small signal behavior of both the modified PLL control structure and the droop control structure, a network with single inverter connected to a load through a transformer and a PI line as shown in Fig. 2 is utilized. Here, transformer impedance $X_{tran} = 8\%$ on the MVA base of the transformer. The PI line is represented by $R_{line} = 0.0017pu, X_{line} = 0.0046pu, B_{line} = 0.033pu$ on a system MVA base of 100 MVA. The load is represented as a constant impedance load with the values of impedance measured at a nominal $1pu$ voltage. The point of interconnection (POI) of the inverter resource is assumed to be the network side of the transformer.

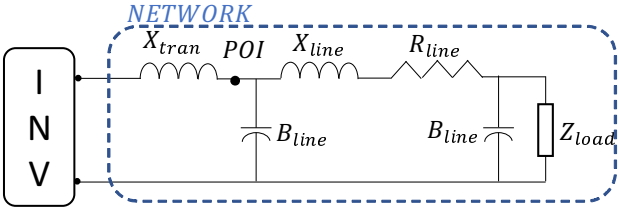

Figure 2. Single inverter - load network to verify similarities in small signal behavior

The values of control gains used in the modified PLL control loop are, $K_{pp}^{inv} = 0.5$, $K_{ip}^{inv} = 20.0$, $\omega_{Drp} = 30.0$, $K_{pv}^{inv} = -0.5$, $K_{iv}^{inv} = -150.0$, $Q_{Drp} = 0.045$, $K_{pv_q}^{inv} = 10.0$, $K_{iv_q}^{inv} = 50.0$, $K_{pod} = 10.0$, $T_{w_{pod}} = 0.01$, $T_{1_{pod}} = 0.01$, $T_{2_{pod}} = 0.001$, $K_{pi} = 0.5$, $K_{ii} = 20.0$, $K_{ppll} = 20.0$, and $K_{ipll} = 700.0$. All quantities within the control loop are in per unit with the exception of the PLL gains. The values of control gains used in the droop loop are, $T_r = 0.01$, $T_f = 0.00001$, $\omega_{Drp} = 30.0$, $T_v = 0.00001$, $Q_{Drp} = 0.045$, $K_{pv}^{inv} = 3.0$, $K_{iv}^{inv} = 10.0$, $K_{pi} = 0.5$, and $K_{ii} = 20.0$. Again all quantities within the control loop are in per unit with the exception of the time constants. For simplicity, only an L filter is assumed with $L_f^1 = 0.15pu$ on the MVA base of the inverter.

Consider a 1000 MVA inverter and a load of 900 MW and 210 Mvar. The inverter control loops are tasked with controlling voltage to a value of $V_{inv}^{ref} = 1.035pu$.

The four right most small signal modes of the system are tabulated in Table 2. The grouping of the modes in Table 2 is not meant to indicate participation of similar state variables. In fact, the participation of states in each mode is not expected to be similar between the modified PLL control method and the droop control method as there are structural differences in the state space representation and controller parameter values. However, the operational inference obtained from the use of both control methods is that of potential stable grid forming behavior in a 100% inverter network.

Table 2. Four right most modes with a 1000 MVA inverter connected to a load of 900 MW and 210 Mvar

Modified PLL control	Droop Control
-0.8207	-2.5499 $\pm$ 0.2042j
-20.9382	
-37.1242	-40.6806 $\pm$ 3.0198j
-40.3516	

Since in a realistic power network, each generation source will be expected to operate in a stable manner across a wide variety of operating points, it can be beneficial to evaluate the extent to which operational similarity between the modified PLL control method and droop control method holds. To carry out this evaluation, P_{load} is varied from 1.0 MW to 1000.0 MW in steps of 10.0 MW. At each value of active power load, Q_{load} is allowed to vary between $\pm\sqrt{S_{INV_{base}}^2 - P_{load}^2}$, again in steps of 10 Mvar. Here, $S_{INV_{base}}$ is the MVA rating of the inverter which is 1000 MVA in this exercise. For each combination of P_{load} and Q_{load}, the active and reactive power output of the inverter is evaluated, assuming again that voltage is controlled at a value of $V_{inv}^{ref} = 1.035pu$. If the absolute value of reactive power required from the inverter is greater than 30% of its rating, the operational scenario is not analysed. This is based on usual inverter operational critera wherein inverter Q_{max} and Q_{min} is $\pm 0.3pu$ of its rating.

The small signal stability of the inverter across these combinations of P_{load} and Q_{load} is shown in Fig. 3. In this figure, a green square is indicative of a stable system with all modes in the left half plane and with every mode having a damping ratio greater than 0.1. A yellow square is indicative of stable system with all modes in the left half plane, but with at least one mode having a damping ratio lower than 0.1. A red square is indicative of an unstable system with at least one mode lying in the right half plane.

It can be seen that both forms of inverter control

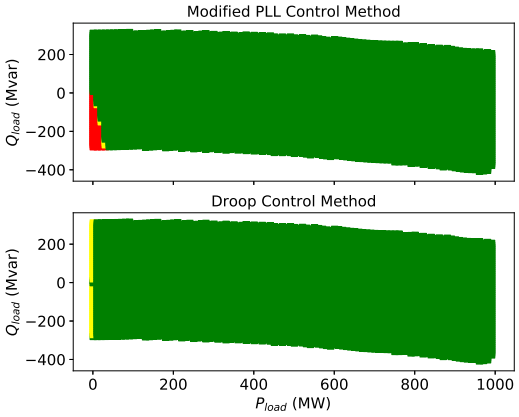

Figure 3. Small signal stability envelope for 1000 MVA inverter connected to load (■- Unstable, ■- Underdamped, ■- Stable)

generally have a similar operational characteristic, from the small signal sense. At low levels of active power output along with capacitive reactive load, both control methods can have challenges with maintaining stability. The modified PLL control method exhibits an instability at higher levels of capacitive reactive load. This behavior could potentially be an obstacle for bringing about blackstart and system restoration. However, through the implementation of additional auxiliary control loops an improvement in stability can be obtained [22].

To verify these operational similarities in time domain, a detailed EMT simulation is carried out at two operating conditions with a time step of $5\mu s$. In this detailed EMT simulation, $L_f^1 = L_f^2 = 0.15pu$, $R_f^1 = R_f^2 = 0.0015pu$, and $C_f = 0.0167pu$ all on the MVA base of the inverter. The operating condition chosen is with $P_{load} = 60MW$ and $Q_{load} = -210Mvar$ and a subsequent 10% increase in load is considered. The time domain response as observed at the POI is shown in Fig. 4.

It can be seen that the operational behavior of the system is similar. We acknowledge that there is a difference in the transient response as the system moves towards its new steady state. The difference in the transient can be explained by structural differences in the state space model of the two control structures along with difference in controller parameterization. However, operationally from a small signal perspective, both control modes achieve the final steady state operating point in a similar fashion, albeit with different rise times. Fitting the rise time within a certain upper limit is definitely possible either through optimal control design and/or adaptive control gain scheduling [22].

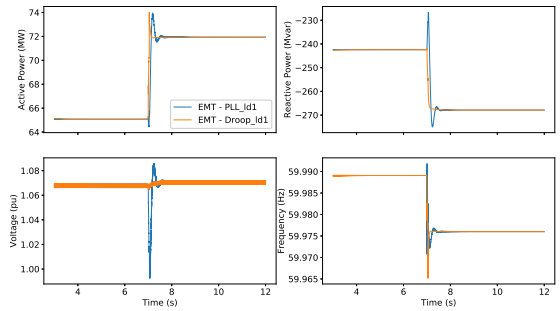

Figure 4. Comparison of EMT time domain response observed at POI for $P_{load} = 60MW$ and $Q_{load} = -210Mvar$ followed by 10% increase in load at $t = 5.0s$

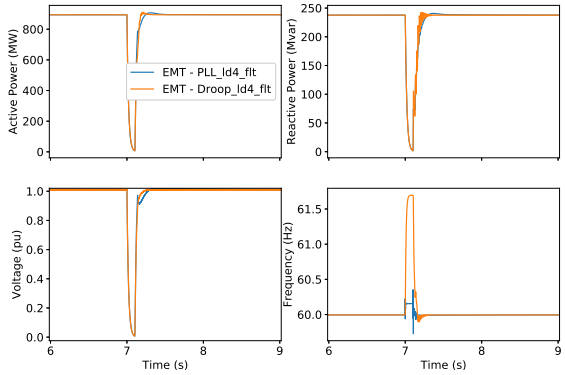

Figure 5. Comparison of EMT time domain response observed at POI for $P_{load} = 900MW$ and $Q_{load} = 210Mvar$ followed by three phase solid fault at POI at $t = 5.0s$

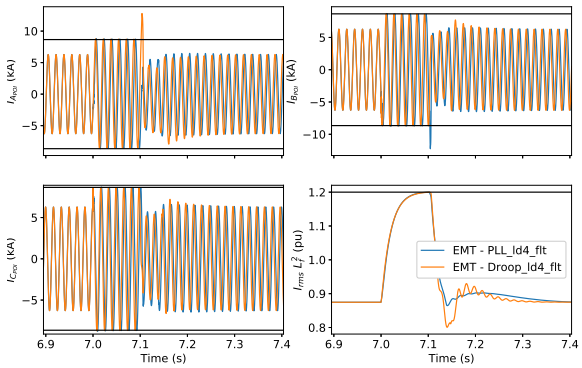

Figure 6. Comparison of EMT time domain current output for $P_{load} = 900MW$ and $Q_{load} = 210Mvar$ followed by three phase solid fault at POI at $t = 5.0s$

The response at the POI for both control methods for a 6-cycle solid to ground three phase fault applied at the POI is shown in Fig. 5. It can be seen that during the fault, the modified PLL control loop restricts the deviation in frequency (and subsequently angle) as compared to the droop control method. However, both control methods are able to successfully ride through the severe fault in a very similar fashion. The output current from the inverter is shown in Fig. 6 with the three phase currents measured at the POI and the per unit RMS current magnitude measured through L_f^2. Both control methods are able to successfully maintain current output within the maximum current limit of 1.2 pu on the inverter MVA base (per phase current limit is the peak value of maximum current). At the time of fault clearing, both control methods result in a sub-cycle spike in current output which is however quickly controlled. The reason for the difference in the spike being in A phase for droop control method and in B phase for modified PLL control method can be attributed to the slight difference in value of frequency (and angle) at the time of fault clearing.

The results from this section showcase the operational similarity that can be achieved across both PLL control methods and other forms of primary droop control schemes. However here, a cautionary note is appropriate. The objective of this analysis is not to state that newer forms of inverter controls may not be required. Continuous research and development is definitely required to further improve ways of controlling inverters in an increased inverter paradigm. Rather, the objective here is to showcase that there are many nuances involved in inverter control methods and various inverter manufacturers can have their own proprietary approach to develop a robust control method. Given that a system planner is ultimately interested in operational performance of an inverter resource, the method of delivery of the operational performance can and should be the purview of the inverter manufacturer. However, this operational similarity allows for the development and creation of universal generic models that can now be parameterized to provide the trend of response of multiple inverter methods.

3.2. Performance of universal model across multiple time scales

To compare the performance of the universal model developed in Section 2.2, a simple network shown in Fig. 7 is used. Here, an equivalent source is initially connected in parallel with the load. The parameters of the PI line and the transformer remain the same as that considered in Section 3.1. The performance across multiple time scales is compared by observing the behavior across both EMT domain and positive sequence domain. EMT domain simulations are again carried out at a simulation time step of $5\mu s$ while

positive sequence simulations are carried out at a time step of $1ms$.

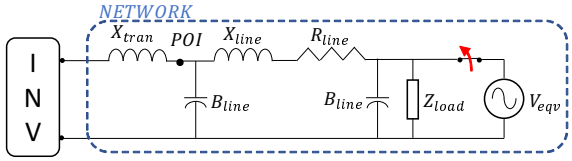

Figure 7. Single inverter - load - equivalent network to showcase behavior of universal inverter model

At the start of the simulation, the inverter is dispatched with $P_{inv}^{ref} = 800MW$ and $V_{inv}^{ref} = 1.035pu$ along with $P_{load} = 900MW$ and $Q_{load} = 210Mvar$. Since the dispatch of the inverter is lower than the total load, the surplus power is provided by the equivalent voltage source. In the inverter controller, except for parameters $K_{pv_q}^{inv}$, $K_{iv_q}^{inv}$, and K_{pod} which were set to zero, the values of all other parameters and elements are kept the same as in Section 3.1. The three parameters were set to zero in order to improve the transient behavior of the modified PLL control method during the grid connected mode (here again an optimal tuning exercise was not carried out to identify exact values for the parameters). At $t = 5.0s$ the breaker connecting the equivalent source to the rest of the circuit is opened thereby creating a 100% inverter network. Following this at $t = 10.0s$ a solid to ground three phase fault is applied at the POI.

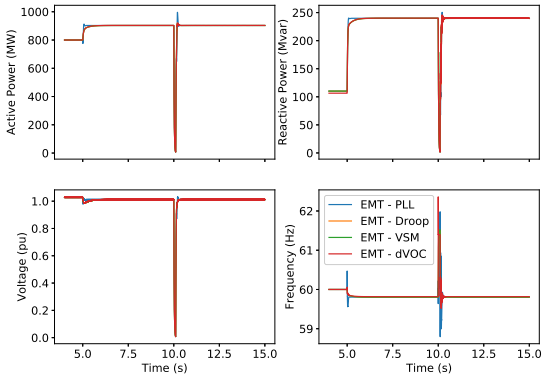

Figure 8. Comparison of EMT time domain response of universal model in different GFM modes for $P_{load} = 900MW$ and $Q_{load} = 210Mvar$ with disconnection of V_{eq} at $t = 5.0s$ followed by three phase solid fault at POI at $t = 10.0s$

A comparison of the response in EMT domain across all four grid forming modes of the universal model is shown in Fig. 8 while a comparison of the response across all four grid forming modes in positive sequence domain is shown in Fig. 10. From both figures

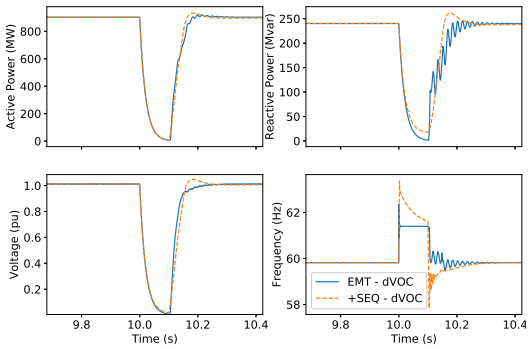

Figure 9. Comparison of EMT and positive sequence time domain response of universal mode in dVOC mode for $P_{load} = 900MW$ and $Q_{load} = 210Mvar$ with disconnection of V_{eq} at $t = 5.0s$ followed by three phase solid fault at POI at $t = 10.0s$

the similarity of the responses can be observed which aligns with the inferences made in the previous section. Further, the transfer of the model from EMT domain to positive sequence domain is achieved with the same values of control parameters.

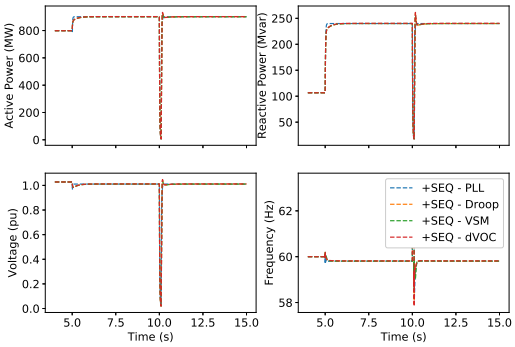

Figure 10. Comparison of positive sequence time domain response of universal model in different GFM modes for $P_{load} = 900MW$ and $Q_{load} = 210Mvar$ with disconnection of V_{eq} at $t = 5.0s$ followed by three phase solid fault at POI at $t = 10.0s$

A one-to-one comparison of the behavior of the dVOC model across both EMT domain and positive sequence domain, for the duration of the fault, is shown in Fig. 9. When the equivalent source is disconnected, initially there is a deficit in generation in the network as the inverter was dispatched at 800 MW. The deficit in generation both from active and reactive power results in voltage and frequency dropping. Subsequently in all grid forming modes, frequency and voltage are controlled with an increase in active power and reactive power output. The response for a subsequent three phase solid to ground fault is also shown. It is seen that across all grid forming modes, both in EMT domain or positive

sequence domain, the response of the universal model is similar and consistent with seamless translation of parameter values.

3.3. Large system with multiple grid forming control types

So far, either a single inverter connected to an equivalent voltage source or an isolated single inverter and load system has been considered. However in any practical power network, there can be different inverter control methods present. To consider such a scenario and to validate the behavior of both the EMT domain and positive sequence domain universal inverter model, the IEEE 14 bus benchmark system topology is used with a few modifications as shown in Fig. 11.

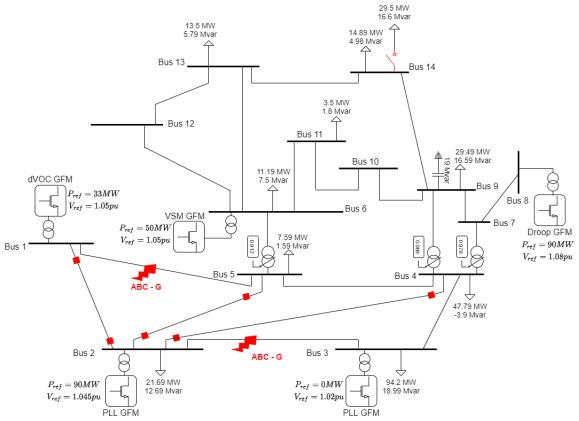

Figure 11. IEEE 14 bus benchmark system topology considered to validate behavior of EMT and positive sequence universal inverter model

Each type of grid forming control method is allocated across the five energy sources of the network. The parameterization of each instance of the model remains the same as in Section 3.2 except for parameter ω_{flag} whose value is set based on the options shown in Fig. 1. The values of active power reference and voltage magnitude reference of each inverter are shown in the figure. Two sets of events are considered: (i) *load event* - switching in of load at bus 14 at $t = 2.0$ followed by switching out of the same load at $t = 5.0s$, and (ii) *fault event* - opening of lines between buses 1-2, 2-4, 2-5 at $t = 4.0s$ followed by a 6 cycle three phase to ground solid fault between buses 2-3 at $t = 5.0s$ and another 6 cycle three phase to ground solid fault between buses 1-5 at $t = 6.0s$.

For the *load event*, the response of inverter at bus 1 and bus 2 is shown in Fig. 12. It is seen that the response both in positive sequence domain and in EMT domain are consistent across control methods. An example of this can be inferred from the reactive power plot immediately after the load change. At bus 2, the reactive power injection immediately moves opposite to the direction of the voltage change. However at bus 1, there is another transient characteristic that is present at the instant of disturbance, and this transient is adequately captured in both simulation domains. A similar match in the trend of response is also observed at each of the other inverter locations.

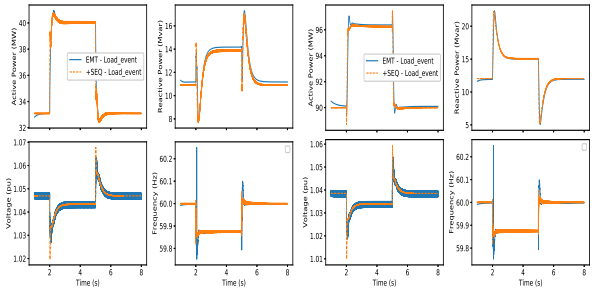

Figure 12. (Left) Response of inverter at bus 1, (right) response of inverter at bus 2 for the load event compared across both EMT domain and positive sequence domain

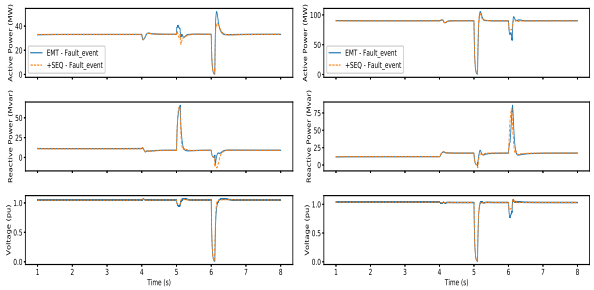

Figure 13. (Left) Response of inverter at bus 1, (right) response of inverter at bus 2 for the fault event compared across both EMT domain and positive sequence domain

For the *fault event*, the response of inverter at bus 1 and bus 2 is shown in Fig. 13. Here once again it can be seen that the response is consistent across both simulation domains. It is acknowledged that the positive sequence model is not completely accurate, especially from the perspective of active power transfer during the fault. However, the model is still able to provide the trend of the response which would be sufficient for use from a transmission planning perspective.

4. Conclusion

This paper has discussed the development, parameterization, and use of a universal generic

grid forming model for future inverter based resources. This generic model has the ability to represent the dynamic behavior of four different grid forming techniques, namely: droop, virtual synchronous machine, dispatchable virtual oscillator, and phase locked loop. Both structural similarity and operational similarity across these different control methods has been exploited to enable the development of the generic model. Further, the model is implemented in both detailed EMT domain and in positive sequence domain with similar results. Such a modeling exercise for grid forming control methods has so far not been reported in research literature. The model from this paper can now allow transmission planners the ability to design and plan the operation of a future system while also providing inverter manufacturers the necessary information for efficient control design. Use of such a universal generic model hence has wide ranging benefits for the power industry and hence the development of the model proposed in this paper is considered to be a significant contribution to the state of the art. Future work includes analysis of the variation in system modes with change in load levels and characteristics, comparison of grid forming start up and synchronization methods, and dynamic performance to unbalanced system conditions.

References

[1] P. Pourbeik *et al.*, "Generic dynamic models for modeling wind power plants and other renewable technologies in large-scale power system studies," *IEEE Transactions on Energy Conversion*, vol. 32, no. 3, pp. 1108–1116, 2017.

[2] D. Ramasubramanian, P. Pourbeik, E. Farantatos, and A. Gaikwad, "Simulation of 100% inverter-based resource grids with positive sequence modeling," *IEEE Electrification Magazine*, vol. 9, no. 2, pp. 62–71, 2021.

[3] P. Kundur, N. J. Balu, and M. G. Lauby, *Power System Stability and Control*. McGraw-Hill, 1994.

[4] Electric Reliability Council of Texas, "2020 Panhandle Regional Stability Study," July 2020.

[5] M. Chandorkar, D. Divan, and R. Adapa, "Control of parallel connected inverters in standalone AC supply systems," *Ind. Appl., IEEE Trans.*, vol. 29, no. 1, pp. 136–143, 1993.

[6] S. D'Arco, J. Suul, and O. Fosso, "A virtual synchronous machine implementation for distributed control of power converters in smartgrids," *Electric Power Systems Research*, vol. 122, pp. 180 – 197, 2015.

[7] M. Lu, S. Dutta, V. Purba, S. Dhople, and B. Johnson, "A grid-compatible virtual oscillator controller: Analysis and design," in *IEEE Energy Conversion Congress and Exposition*, pp. 2643–2649, 2019.

[8] D. B. Rathnayake, M. Akrami, C. Phurailatpam, S. P. Me, S. Hadavi, G. Jayasinghe, S. Zabihi, and B. Bahrani, "Grid forming inverter modeling, control, and applications," *IEEE Access*, vol. 9, pp. 114781–114807, 2021.

[9] M. Li, Y. Wang, W. Hu, S. Shu, P. Yu, Z. Zhang, and F. Blaabjerg, "Unified modeling and analysis of dynamic power coupling for grid-forming converters," *IEEE Transactions on Power Electronics*, vol. 37, no. 2, pp. 2321–2337, 2022.

[10] W. Du, F. K. Tuffner, K. P. Schneider, R. H. Lasseter, J. Xie, Z. Chen, and B. Bhattarai, "Modeling of grid-forming and grid-following inverters for dynamic simulation of large-scale distribution systems," *IEEE Transactions on Power Delivery*, vol. 36, no. 4, pp. 2035–2045, 2021.

[11] B. Johnson, T. Roberts, O. Ajala, A. D. Dominguez-Garcia, S. Dhople, D. Ramasubramanian, A. Tuohy, D. Divan, and B. Kroposki, "A generic primary-control model for grid-forming inverters: Towards interoperable operation & control," in *2022 55th Hawaii International Conference on System Sciences (HICSS), Maui, HI, USA*, pp. 1–10, 2021.

[12] North American Electric Reliability Corporation, "Reliability Guideline: Performance, Modeling, and Simulations of BPSConnected Battery Energy Storage Systems and Hybrid Power Plants," March 2021.

[13] John Schmall, "IBR Damping Support Revision Request Update." [Online]: `http://www.ercot.com/content/wcm/key_documents_lists/205465/4._IBR_Damping_Aug_RIW.pdf`, Aug. 2020.

[14] "Grid Forming Inverters for Increase in Inverter Based Resource Percentage," Tech. Rep. 3002020786, EPRI, Palo Alto, CA:, 2021.

[15] D. Ramasubramanian, "Differentiating between plant level and inverter level voltage control to bring about operation of 100% inverter based resource grids," *Electric Power Systems Research*, vol. 205, no. 107739, 2022.

[16] D. Ramasubramanian, W. Baker, J. Matevosyan, S. Pant, and S. Achilles, "Asking for fast terminal voltage control in grid following plants could provide benefits of grid forming behavior," *IET Generation, Transmission & Distribution*, 2022.

[17] D. Ramasubramanian, "Importance of considering plant ramp rate limits for frequency control in zero inertia power systems," in *2021 IEEE Green Technologies Conference (GreenTech)*, pp. 320–322, 2021.

[18] R. K. Varma and H. Maleki, "Pv solar system control as statcom (pv-statcom) for power oscillation damping," *IEEE Transactions on Sustainable Energy*, vol. 10, no. 4, pp. 1793–1803, 2019.

[19] R. K. Varma and M. Akbari, "Simultaneous fast frequency control and power oscillation damping by utilizing pv solar system as pv-statcom," *IEEE Transactions on Sustainable Energy*, vol. 11, no. 1, pp. 415–425, 2020.

[20] "Concorda Positive Sequence Load Flow Software (PSLF)." General Electric International, Inc., 2021.

[21] D. Ramasubramanian *et al.*, "Positive sequence voltage source converter mathematical model for use in low short circuit systems," *IET Generation, Transmission Distribution*, vol. 14, no. 1, pp. 87–97, 2020.

[22] T. Chen, O. Dutta, D. Ramasubramanian, and E. Farantatos, "An LQR-based Robust Grid Forming Inverter Controller for Black Start Applications," in *2021 IEEE Power & Energy Society ISGT Asia Conference*, 2021.